IEEE Access
Multidisciplinary ⋮ Rapid Review ⋮ Open Access Journal

Received December 22, 2019, accepted January 24, 2020, date of publication January 29, 2020, date of current version February 12, 2020.

Digital Object Identifier 10.1109/ACCESS.2020.2970219

Skin Temperature Elevation for Incident Power Densities From Dipole Arrays at 28 Ghz

TAKUMA NAKAE[1], DAISUKE FUNAHASHI[1], JUNJI HIGASHIYAMA[2], (Member, IEEE), TERUO ONISHI[2], (Member, IEEE), AND AKIMASA HIRATA[1,3], (Fellow, IEEE)

[1]Department of Electrical and Mechanical Engineering, Nagoya Institute of Technology, Nagoya 466-8555, Japan
[2]NTT DOCOMO, Inc., Kanagawa 239-8536, Japan
[3]Center of Biomedical Physics and Information Technology, Nagoya Institute of Technology, Nagoya 466-8555, Japan

Corresponding author: Akimasa Hirata (ahirata@nitech.ac.jp)

This work was supported by the Ministry of Internal Affairs and Communications, Japan (TN, DF, and AH).

ABSTRACT The relationship between skin temperature elevation and incident power density (IPD) from radio-frequency near-field exposure at 28 GHz for different angles of incidence is evaluated computationally in this study. The averaging scheme of the IPD is crucial for determining the maximum allowable exposure levels of wireless equipment to comply with certain standards/regulations. However, it is still unclear which component of the IPD (i.e., the norm or normal component to the human body) is more related the temperature elevation. In the case of four-element dipole arrays, the distances between the model and the antenna were 15 and 30 mm in transverse-electric- and transverse-magnetic-like polarized waves, respectively, and in the case of eight-element dipole arrays, the distances were 45 mm from the center of the array. From our computational results for four- and eight-element dipole arrays, we confirmed that the normal component of the IPD provides better correlation with the surface skin temperature, regardless of angle of incidence, particularly for smaller angles of incidence ($<30°$). The enhancement of the ratio of the temperature increase to IPD was observed around the Brewster's angle, which is mainly attributable to the difference in transmittance at the body surface. This exposure scenario may not occur as the antenna–human distance was too large to consider compliance at the closest distance. In terms of output power, the most restrictive condition for compliance is shown to be normal incidence, suggesting the importance of compliance for such exposure scenarios. Furthermore, the absorbed power density proved to be an appropriate metric to monitor in relation to skin temperature elevation.

INDEX TERMS Radiation safety, standardization, 5th generation wireless communication.

I. INTRODUCTION

To develop transmission quality in millimeter wave bands, an antenna array may be implemented on mobile terminals in 5th-generation (5G) wireless communication systems [1], [2]. Radio waves emitted from terminals form a beam whose direction changes with time. In 5G transmission system development, a key factor is human safety [3]–[12]. Joint working groups of IEC Technical Committee (TC) 106 and IEEE/ICES TC34 have been standardizing assessment methods for near-field exposure of products above 6 GHz.

The assessment methods are based on international exposure guidelines/standards for human protection, which have been revised recently (both IEEE and ICNIRP) [13]–[16]. At frequencies higher than 100 kHz, potential adverse health effects are thermally induced or caused by temperature elevation [15]–[17]. To prevent excess skin temperature elevation, surrogate internal electrical quantities and their corresponding external field strengths/power densities have been prescribed in the guidelines/standards. In frequency ranges above 6 GHz, including 28 GHz, which is the frequency band assigned to 5G, absorbed or epithelial power density (APD) [18] and incident power density (IPD) are used for basic restrictions and reference levels for local exposure, respectively [13], [16]. These metrics correspond to internal and external physical quantities, where the latter is conservatively derived from the former. Recently, the surface temperature elevation for radio-frequency (RF) exposure from 5G devices or at the corresponding frequencies (especially

The associate editor coordinating the review of this manuscript and approving it for publication was Mohammad Tariqul Islam.

around 28 GHz) has been computed by different groups (e.g., [19]–[24]).

A two-dimensional analytical solution suggests that almost all energy is deposited for transverse-magnetic (TM) mode exposures at an angle of incidence equal to Brewster's angle [25]; for biological tissues, this angle ranges from 65 to 80° [22], [26]. Therefore, the power deposited in a human would be enhanced compared with the power at normal incidence [22], [26]. However, only a few studies [19], [27], [28] have computed the relationship between IPD and surface temperature elevation in 3-D local exposure scenarios but not for different incident angles, although this relates better to the rationale for relating the exposure guidelines and product safety standards. Furthermore, the effectiveness of APD should be confirmed for additional cases [19], [20].

In this study, we computed the relationship between skin temperature elevation and IPD averaged over different definitions for RF exposure from dipole arrays. The rationale for considering two different definitions is that a detailed procedure for assessing compliance is beyond the scope of the exposure guidelines/standards (ICNIRP and IEEE C95.1 standards). Instead, it is the role of the standardization bodies (IEC TC 106 and IEEE ICES TC34) to complete the product safety assessment based on the exposure guidelines/standards. In the IEEE ICES TC95 meeting, it was discussed that additional comments would be help establish a relation relate between them, when possible, in the next revision of IEEE C95.1 standard. For this purpose, relatively simple exposure scenarios will be considered, similar to the international exposure guidelines/standard [13], [16]. Exposures with TE- and TM-like polarizations are considered, and the effectiveness of APD at different angles of incidence to the human body is discussed.

II. MODELS AND METHODS

A. SKIN BODY MODEL

A three-dimensional homogeneous cube with thermal parameters and the dielectric properties of skin was considered as the model for skin. The dielectric properties of the skin were determined with a four-Cole–Cole dispersion model [29]. The depth, side length, and height of the homogeneous cubic skin model were 75, 225, and 150 mm, respectively.

Such a simplified model is often used in discussions of millimeter waves, as in the international exposure guidelines/standard [13], [16] and in working group 5 under IEEE ICES TC95 SC6. These dimensions were chosen to imitate the head size, with a truncation in the depth (75 mm). The model dimensions are large enough not to perturb the results.

B. ELECTROMAGNETIC COMPUTATION

For electromagnetic analysis, our in-house code of the finite-difference time-domain method [30] was used. The resolution of the model was chosen to be 0.25 mm to satisfy the Courant condition at approximately 28 GHz (see Sec. II. D for exposure scenarios).

The IPD and APD were averaged over an area of 4 cm^2, as described in the IEEE C95.1-2019 standard [13] and the ICNIRP RF guidelines [16]. The IPD averaged with different definitions was computed in this study; the norm and the normal component against the surface of model are defined by Eqs. (1) and (2), respectively.

$$|\boldsymbol{S}| = \frac{1}{2}\left|\mathrm{Re}\left(\boldsymbol{E}\times\boldsymbol{H}^*\right)\right|, \tag{1}$$

$$S_n = \frac{1}{2}\iint_A \mathrm{Re}\left(\boldsymbol{E}\times\boldsymbol{H}^*\right)\cdot\boldsymbol{ds}/A, \tag{2}$$

where $\boldsymbol{E}$, $\boldsymbol{H}$, $\boldsymbol{ds}$, and A represent the electric field, magnetic field, integral variable vector with normal direction, and integral area to the model surface, respectively. Eq. (1) is the definition of IPD that is mentioned in the international guidelines. Eq. (2), which is being discussed in working group 5 under IEEE ICES TC95 as well as in IEC TC106, has been considered for comparison to relate with the surface temperature elevation, in addition to practical purposes. APD is defined as the power deposited in the human body.

$$APD(x,y) = \frac{1}{2}\int \sigma(\boldsymbol{r})\,|\boldsymbol{E}(\boldsymbol{r})|^2\,dz, \tag{3}$$

where z and σ represent the direction perpendicular to the body surface and the electric conductivity of the tissue at position $\boldsymbol{r}$, respectively.

C. THERMAL COMPUTATION

The temperature increase in the human model as a result of power deposition was computed by solving a bioheat transfer equation [31]. A generalized equation that considers various heat exchange mechanisms such as heat conduction, blood perfusion, and microwave-induced heating, is represented by the following equation:

$$C(\boldsymbol{r})\rho(\boldsymbol{r})\frac{\partial T(\boldsymbol{r},t)}{\partial t} = \nabla\cdot(K(\boldsymbol{r})\nabla T(\boldsymbol{r},t)) + \rho(\boldsymbol{r})SAR(\boldsymbol{r}) + M(\boldsymbol{r},t) - B(\boldsymbol{r},t)\,(T(\boldsymbol{r},t) - T_B(\boldsymbol{r},t)) \tag{4}$$

where T is the tissue temperature, T_B is the blood temperature, C, K, M, and B are the specific heat, thermal conductivity, metabolic heat generation, and blood perfusion term, respectively, ρ is the mass density of the tissue, and t is the time variable.

For local exposure where the power absorption from the source (typically on the order of a few hundred milliwatts or less) is much smaller than the basal metabolic rate ($\sim$ 100 W), the blood temperature can be assumed to be spatiotemporally constant at 37 °C. This is because the energy dose is insufficient to cause core temperature elevation through blood temperature elevation. Similarly, assuming that the skin temperature elevation is not high enough to activate thermoregulation, the value of the blood perfusion

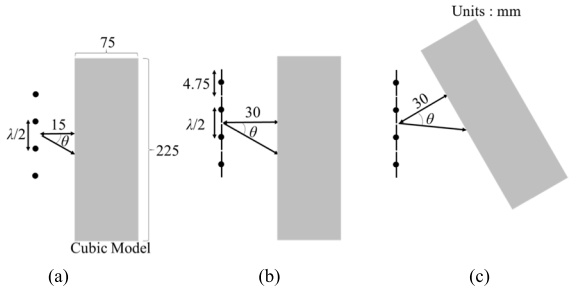

FIGURE 1. Homogeneous cubic model exposure from four-element dipole antenna arrays: arrangement of (a) TE-like, (b) TM-like, and (c) TM-like (inclined model) polarizations. The cubic model was not considered in calculating the incident power density.

term is assumed to be constant. The boundary condition for Eq. (4) is subsequently expressed as

$$-K(r)\frac{\partial T(\mathbf{r},t)}{\partial n} = H \cdot (T_s(\mathbf{r},t) - T_e(t)), \tag{5}$$

where H, T_s, and T_e denote the heat transfer coefficient, surface temperature of the tissue, and ambient temperature (independent of the position), respectively. The variable n denotes the axis perpendicular to the model surface. The bioheat transfer equation subjected to the boundary condition was solved to obtain the thermal steady-state temperature elevation. The left-hand side of Eq. (4) was subsequently equated to zero, and all the terms on the right-hand side were treated as independent of t. Most of the thermal parameters used in this study were the same as those used in [32], wherein the parameters were borrowed primarily from the study conducted by [33].

D. EXPOSURE SCENARIOS

Figure 1 shows the near-field exposure scenarios considered in this study: four-element half-wave dipole antenna arrays aligned vertically [Fig. 1(a)] and horizontally [Fig. 1(b)]. The length of the antennas was chosen as 4.75 mm so that they would resonate at 28 GHz. The fields emitted from the vertical and horizontal arrays correspond to TE- and TM-like polarizations, respectively. It is noteworthy that the TE- and TM-like polarized waves are defined as waves whose electric or magnetic field, respectively, is vertical to the plane of incidence. In TM-like polarization, we considered an exposure scenario with the homogeneous cubic model inclined against the line of antennas [Fig. 1(c)] to realize a larger angle of incidence. The separation distances between the model surface and antenna arrays were chosen to be 15 and 30 mm in TE- and TM-like polarized waves, respectively, such that they would not touch each other. The scenario without the cubic model was also considered to calculate IPD. In the ICNIRP guidelines [16], it is stated that "*As a rough guide, distances* $> 2D^2/\lambda[m]$, *between* $\lambda/2\pi$ *and* $2D^2/\lambda[m]$, *and* $< \lambda/2\pi[m]$ *from an antenna correspond approximately to the far-field, radiative near-field and reactive near-field respectively, where D and* λ *refer to the longest dimension of the antenna and wavelength respectively.*" Based on the above-mentioned guidelines, extremely short distances were considered outside the scope of this study. Also, for a small distance of the single dipole, the power absorption may be concentrated around the feeding point. However, the discussion of such cases would be centered on the effectiveness of the metric for an internal physical quantity, i.e., absorbed power density, which is also outside the scope of this study. In addition, for very small antenna array–model separation, the beam may not be formed.

A sinusoidal wave at a frequency of 28 GHz was excited at each feed point, and the radiation direction was changes according to the phase difference between the antenna elements, which is represented by the following equation:

$$\varphi_i = -(i-1)kd\cos\phi, \tag{6}$$

where φ, i, k, d, and ϕ represent the initial phase, the number of antennas, wave number, antenna separation, and the beam direction, respectively. Because the impedance of the antenna varies with the phase difference, the feeding current of the antenna was adjusted so that the total output power of the array was 1 W.

In the TE-like polarized wave, the beam direction at the model surface was adjusted from 0 to 60° in 15° intervals, whereas it was adjusted from 0 to 60° in 15° intervals and at 75 and 80° for the TM-like polarized wave.

III. RESULTS

Figures 2 and 3 show the distributions of the Poynting vector modulus, power deposition, and temperature elevation on the plane crossing the feed points of the four-element dipole antenna array from TE-like and TM-like polarization exposures, respectively. The Poynting vector modulus and power deposition are the values obtained from Eqs. (1) and (3), respectively. The distributions were normalized at the corresponding spatial maximum value at the model surface. The minimum distance from the center of the antenna array to the model surface was 15 mm for TE-like polarization. Figure 3 also presents the Poynting vector modulus for the case where the cubic skin model is inclined to realize a higher angle of incidence. The minimum distance from the center of the antenna array to the model surface was 30 mm for TM-like polarization. From the simulation, the actual distances from the center of the array to the exposed region and its incidence angle from the Poynting vector modulus distribution are also shown in Figs. 2 and 3. Note that the incidence angle in Fig. 3 is defined as the spatial peak power density at the surface where the model exists, even though the spatial distribution of power density is smooth in general.

As shown in Figs. 2 and 3, a side lobe appeared at 45°, which became more apparent with the increase in incidence angle. Similarly, at larger incidence angles, some ripples were observed in the power deposition distribution. The distribution of temperature elevation is similar to that of power deposition, but it is smoother owing to heat conduction. These tendencies are the same for the TM-like polarization, except that the side lobe is more apparent for higher incidence

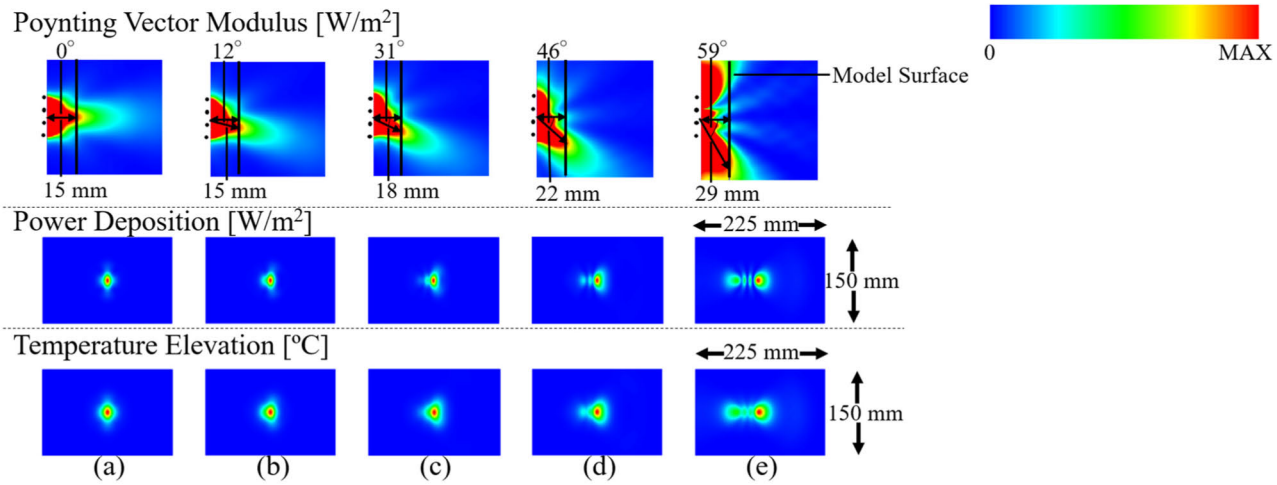

FIGURE 2. Power density distribution, power deposition, and temperature elevation for TE-like polarized wave from four-element dipole antenna array: beam direction of (a) 0, (b) 15, (c) 30, (d) 45, and (e) 60°.

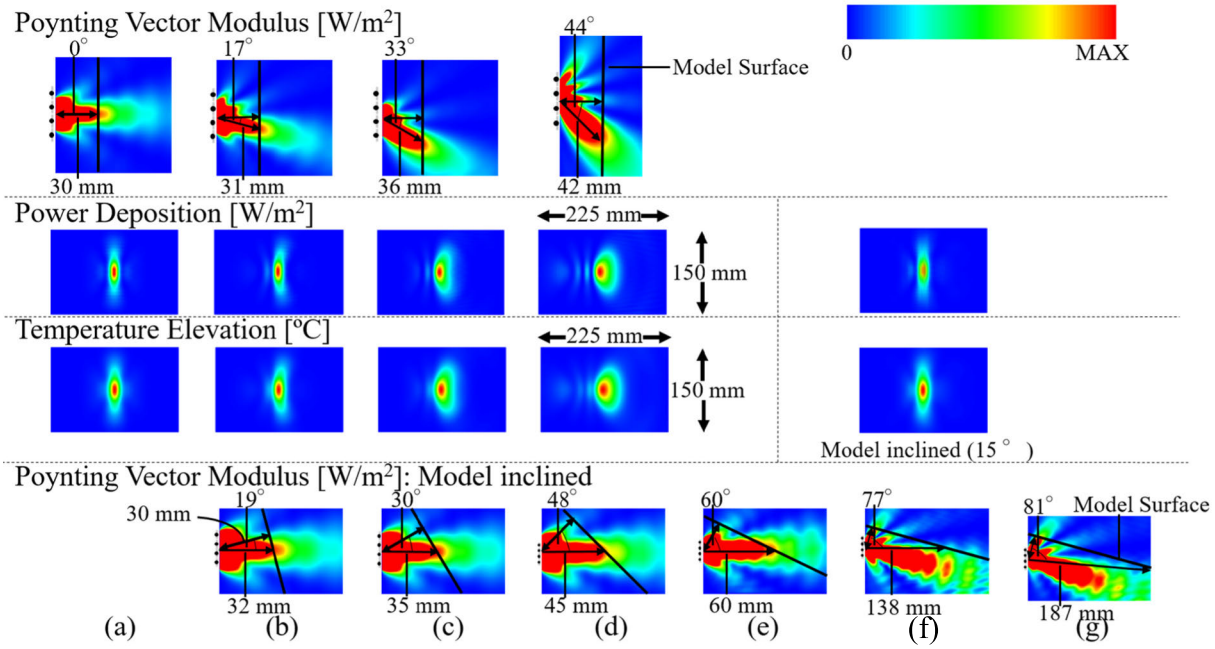

FIGURE 3. Power density distribution, power deposition, and temperature elevation for TM-like polarized wave from four-element dipole antenna array: beam direction of (a) 0, (b) 15, (c) 30, (d) 45, (e) 60, (f) 75, and (g) 80°. The beam angle (theoretical) and computed value at the model surface may differ by up to 4°. The power deposition and temperature elevation for the model inclined at 15° are shown for clarifying the effect of model incline.

angles. The power deposition and temperature elevation distribution between models with or without incline are also close to each other (see Fig. 3). Some difference would be caused by coordinate transformation.

Figures 4 and 5 show the heating factors, defined as the ratio of the maximum surface temperature elevation to the IPD or APD, at different beam directions for TE- and TM-like polarized waves, respectively. In this study, we evaluated the peak power density of the main lobe for a proper comparison.

As shown in Fig. 4, the heating factor of the normal component of the Poynting vector, S_n, depends marginally on the beam direction, whereas that of $|\boldsymbol{S}|$, the norm of the Poynting vector, decreases with the increase in the angle in the TE-like polarized waves. As shown in Fig. 5, the heating factor of S_n increased by a factor of two with increasing incidence angle, which is attributable to the larger transmittance (see black line in Fig. 5). The heating factor of the norm of the Poynting vector matches that of the normal component when

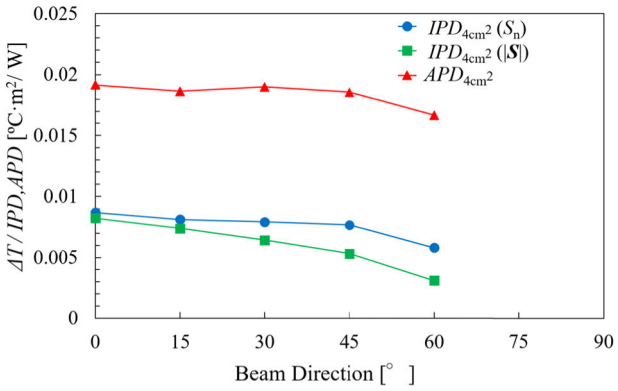

FIGURE 4. Heating factor for different beam directions in TE-like polarized waves.

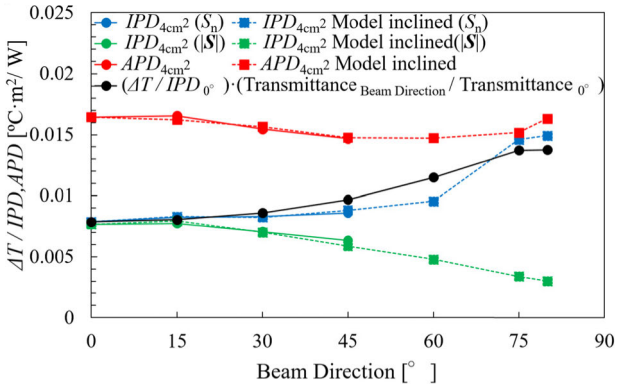

FIGURE 5. Heating factor for different beam directions in TM-like polarized waves. The heating factor compensated for by the transmittance difference is also plotted for comparison.

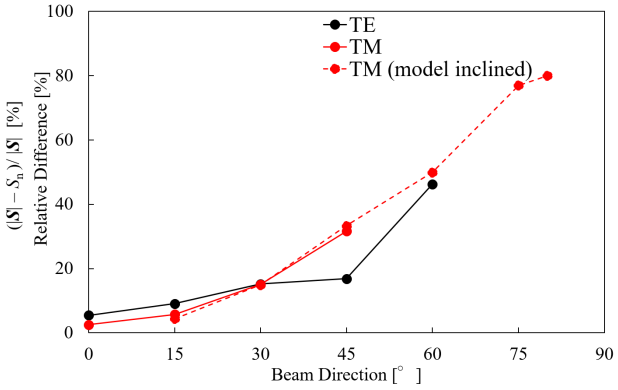

FIGURE 6. Relative difference between norm and normal component of IPD averaged over a square area of 4 cm^2

the angle of incidence is 0° because of compensation by the transmittance.

Figure 6 shows the relative differences of the IPD computed with Eqs. (1) and (2). From this figure, the difference was less than 20% in TE- and TM-like exposures at incidence angles no larger than 30°.

Figures 7 and 8 show the modulus distributions of the Poynting vector, power deposition, and temperature elevation for TE- and TM-like polarizations, respectively, for an eight-element dipole array. The number of antenna elements was determined by practical considerations (e.g., [34]). The separation distance between the model surface and the antenna array was chosen as 45 mm. This separation distance is different from that of the four-element array because a larger distance is needed to form a beam at the model surface. From Figs. 7 and 8, side lobes are observed, and the distribution of temperature elevation is smoother than that of power deposition, as described for the four-element dipole array. Unlike the four-element dipole array, we can see that the distance to form the beam is greater for the eight-element array.

Figs. 9 and 10 show the heating factors for TE- and TM-like polarized waves, respectively. At smaller incident angles, the heating factor is almost the same as that for the four-element dipole array for the TE- and TM-like polarization. However, around the Brewster angle, the heating factor becomes twice as much mainly because of higher transmittance at higher incident angles.

Figure 11 shows the power fed to the antenna array to increase the skin temperature elevation by 1 °C. As shown in the figure, the power required for a constant temperature elevation increases with increasing incidence angle. This is partly supported by the modulus of the Poynting vector in Figs. 3 and 8 in that most of the power at a large incidence angle is not incident on the homogeneous cubic model; instead, it is radiated into free space.

IV. DISCUSSION

The relationship between skin temperature elevation and IPD averaged over different definitions for exposure with different incidence angles was computed in this study. In this study, a homogeneous cube model, which is simple but often used as a canonical model in the international guidelines/standard, was considered for clarifying the effect of incident angle on the heating factors. For normal incidence, the heating factor of our computation of 0.08 °C·m^2/W is in good agreement with those computed in previous studies (0.07–0.12 °C·m^2/W) [21], [18], [35], [36]. However, these values are somewhat larger than those reported experimentally due to the limited exposure area for realistic antennas (0.03 °C·m^2/W) [10].

For TE-like wave exposure from a four-element antenna array, the heating factor S_n depends less on the beam angle as compared with $|\boldsymbol{S}|$ (Fig. 4). The heating factor S_n for TM-like exposure increased by a factor of two around Brewster's angle (Fig. 5), which corresponds to an increase in transmittance. Even for the eight-element antenna array, the heating factors S_n and $|\boldsymbol{S}|$ decreased with increasing angle for the TE-like polarized wave; the heating factors for the four- and eight-element dipole arrays were almost identical (Figs. 9 and 10).

Additionally, for TM-like exposures, the definition of the norm $|\boldsymbol{S}|$ did not exceed the value above the normal incidence.

Around the incidence angle of 60–80° (close to Brewster's angle), the heating factor for the TM-like exposure increased because of the definition of the normal component of the

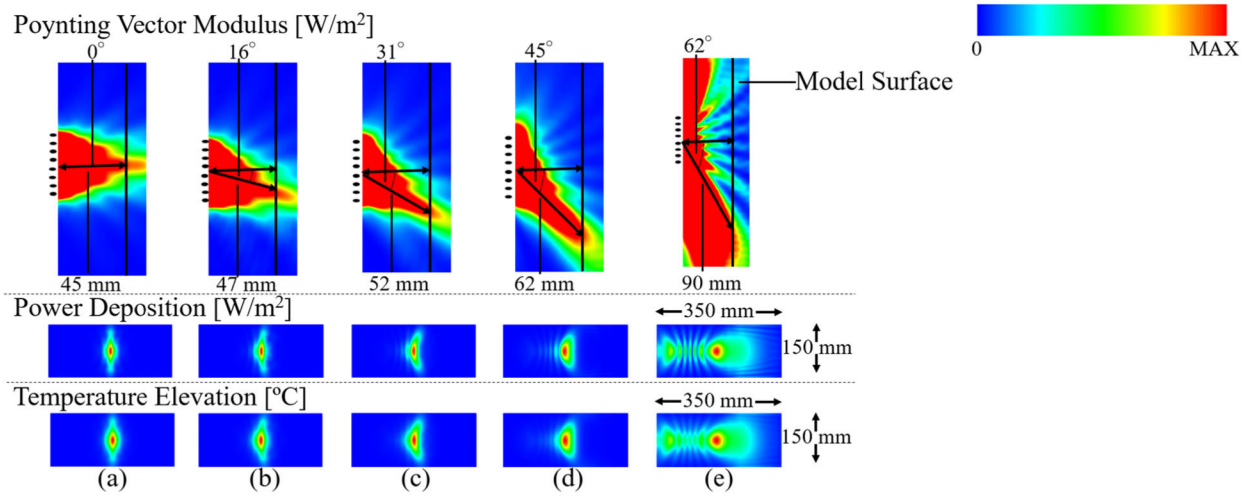

FIGURE 7. Power density distribution, power deposition, and temperature elevation for TE-like polarized wave from eight-element dipole antenna array: beam direction of (a) 0, (b) 15, (c) 30, (d) 45, and (e) 60°.

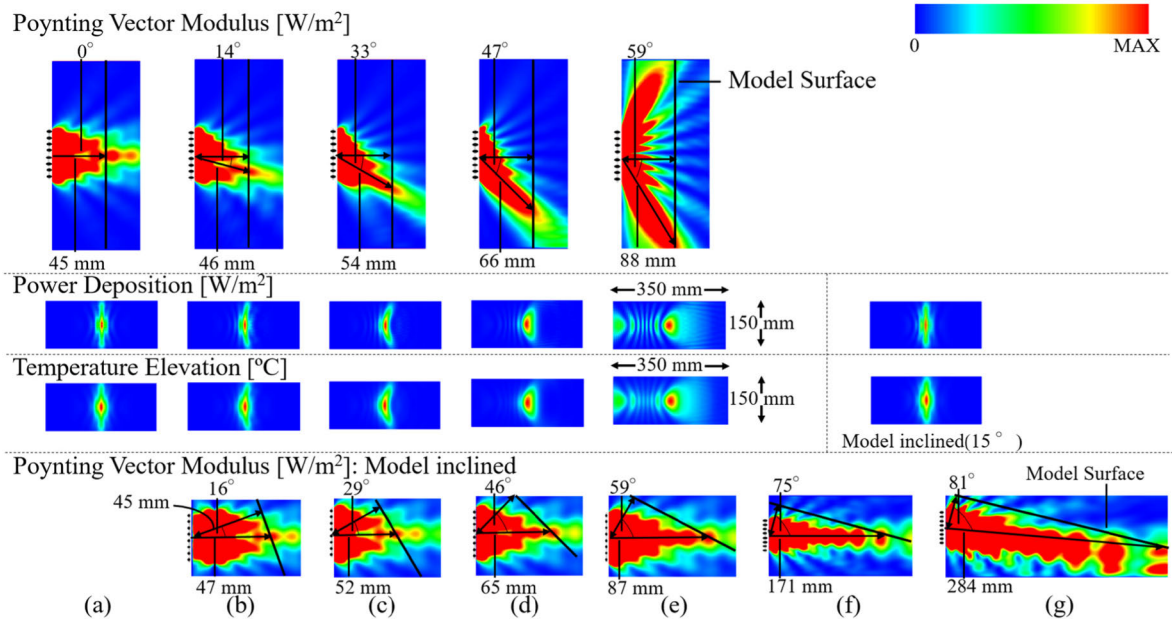

FIGURE 8. Power density distribution, power deposition, and temperature elevation for TM-like polarized wave from four-element dipole antenna array: beam direction of (a) 0, (b) 15, (c) 30, (d) 45, (e) 60, (f) 75, and (g) 80°. The beam angle (theoretical) and computed value at the model surface may differ by up to 4°. The power deposition and temperature elevation for the model inclined at 15° are shown to clarify the effect of model incline.

beam, which is always smaller than the norm. For conservative compliance, the IPD in the propagation beam should be decreased by a factor of up to two (an inverse of cosine at 60°) to obtain a conservative heating factor. At beam directions lower than 60°, the power transmittance decreased and increased by 40% for TE- and TM-like polarizations, respectively [26]. In contrast, the heating factor S_{n} decreased and increased by 30% for TE- and TM-like polarizations, respectively. The reason for this difference is that the angle of a more realistic beam is difficult to define, unlike a two-dimensional plane wave. This is also a reason for the differing heating factor between the four- and eight-element dipole arrays.

The computed heating factor of the IPD is larger for the norm as the definition of the normal component ignores non-normal components. Thus, the heating factor for the normal components is larger but at incidence angles larger than 30°. This suggests that, for practical exposures, these two definitions are almost identical and are theoretically the same value for plane wave exposures. From Fig. 5, the difference in heating factor between models inclined and not inclined was less than 10% for the APD, S_n, and $|\boldsymbol{S}|$, which is primarily caused by the discretization of the model. The heating factor for the APD is insensitive to the incidence angle and is larger than those of the normal component and norm of the IPD. The differences in the

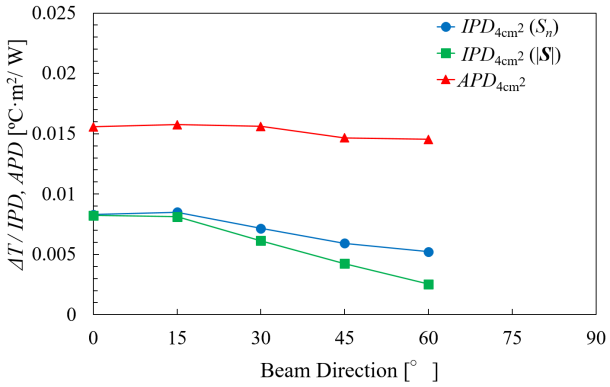

FIGURE 9. Heating factor for different beam angles in TE-like polarized waves in eight-element dipole antenna array.

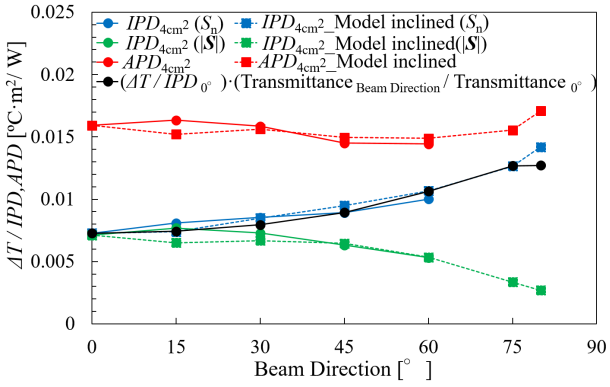

FIGURE 10. Heating factor for different beam angles in TM-like polarized waves in eight-element dipole antenna array.

APD and IPD are attributable to the reflection at the skin surface.

The difference in heating factor of the APD at beam directions from 0 to 75° is less than 20%, as shown in Figs. 4 and 5, which is caused by the differing power deposition distributions. This is consistent with the results of a previous study [18]. Specifically, the power deposited in the surrounding area of the averaging region (4 cm^2) can diffuse to a few centimeters [27]. It is noteworthy that one-half of the side length of the averaging area of 1 cm approximately corresponds to the heat diffusion length (63% decrease from the peak value) [37], [38].

Li, et al. [26] and Samaras and Kuster [22] considered a two-dimensional infinite slab and subsequently reported a larger heating factor at a larger incidence angle for TM-like exposure. This tendency was confirmed in a three-dimensional analysis, as shown in Figs. 5 and 10. Furthermore, we investigated the power required for temperature elevation, which cannot be discussed in a two-dimensional analysis. It was evident from Fig. 11 that the most restrictive case is the case of normal incidence, where the heating factor is not always the largest. As mentioned above, this is because part of the energy is radiated into free space instead of being absorbed by the human model. In addition to the power density of the normal component being small with cosine-θ,

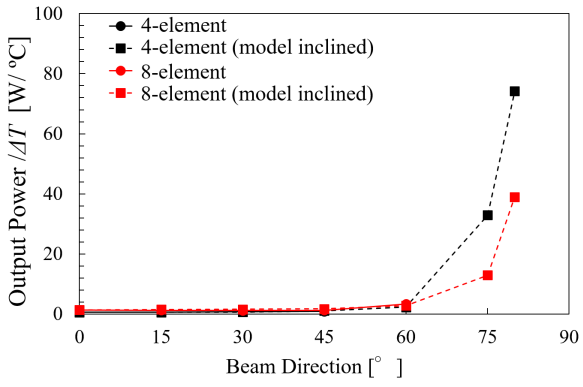

FIGURE 11. Power fed to the antenna array to increase the skin temperature by 1 °C in the case of TM-like exposure.

where θ is the incidence angle, the power emitted from the antenna is the same.

In this study, the uncertainty in dielectric properties and thermal properties on the heating factor was not considered because they may only marginally affect the angle dependence of the heating factor. Recently, new measured data for skin dielectric properties have been reported [39], and the uncertainty caused by dielectric properties on the skin temperature elevation was 6%. The uncertainty was 1.3–2.8 times when including the ambient condition [21], [40], [41]. It is noteworthy that the uncertainties caused by dielectric properties are smaller than the skin thickness and thermal constant (especially for blood).

V. CONCLUSION

The relationship between skin temperature elevation and IPD averaged over different definitions for RF near-field exposure with different polarizations was computed in this study. The distances were 15 and 30 mm in TE- and TM-like polarized waves, respectively, in the case of four-element dipole arrays, and 45 mm in the case of eight-element dipole arrays. These distances were chosen to form a beam at the model surface. The computational results indicated obvious enhancement in the heating factor by a factor of two for the normal component of the IPD, mainly due to the transmittance at the Brewster angle. However, this exposure scenario may not occur, as the antenna–human distance was too large to consider compliance at the closest distance. The most restrictive factor in terms of output power was the normal incidence. This was because the power radiated in free space could not be considered in a two-dimensional analysis. Thus, we conclude that the normal component of the IPD could be used as a metric for practical near-field compliance. Finally, the APD was demonstrated to be an appropriate metric, even for the scenario considered in this study.

REFERENCES

[1] T. S. Rappaport, S. Sun, R. Mayzus, H. Zhao, Y. Azar, K. Wang, G. N. Wong, J. K. Schulz, M. Samimi, and F. Gutierrez, "Millimeter wave mobile communications for 5G cellular: It will work!" *IEEE Access*, vol. 1, pp. 335–349, 2013.

[2] C.-X. Wang, F. Haider, X. Gao, X.-H. You, Y. Yang, D. Yuan, H. Aggoune, H. Haas, S. Fletcher, and E. Hepsaydir, "Cellular architecture and key technologies for 5G wireless communication networks," *IEEE Commun. Mag.*, vol. 52, no. 2, pp. 122–130, Feb. 2014.
[3] T. Wu, T. S. Rappaport, and C. M. Collins, "Safe for generations to come: Considerations of safety for millimeter waves in wireless communications," *IEEE Microw.*, vol. 16, no. 2, pp. 65–84, Mar. 2015.
[4] K. R. Foster, M. C. Ziskin, and Q. Balzano, "Thermal modeling for the next generation of radiofrequency exposure limits: Commentary," *Health Phys.*, vol. 113, no. 1, pp. 41–53, 2017, doi: 10.1097/hp.0000000000000671.
[5] A. Hirata, "Review on human dosimetry for radio-frequency exposure above 6 GHz-international exposure standards," in *Proc. Asia–Pacific Microw. Conf. (APMC)*, Nov. 2018, pp. 681–683.
[6] A. Hirata, D. Funahashi, and S. Kodera, "Setting exposure guidelines and product safety standards for radio-frequency exposure at frequencies above 6 GHz: Brief review," *Ann. Telecommun.*, vol. 74, nos. 1–2, pp. 17–24, Feb. 2019.
[7] M. C. Ziskin, S. I. Alekseev, K. R. Foster, and Q. Balzano, "Tissue models for RF exposure evaluation at frequencies above 6 GHz," *Bioelectromagnetics*, vol. 39, no. 3, pp. 173–189, Apr. 2018.
[8] D. Colombi, B. Thors, and C. Tornevik, "Implications of EMF exposure limits on output power levels for 5G devices above 6 GHz," *IEEE Antennas Wireless Propag. Lett.*, vol. 14, pp. 1247–1249, 2015.
[9] B. Thors, D. Colombi, Z. Ying, T. Bolin, and C. Tornevik, "Exposure to RF EMF from array antennas in 5G mobile communication equipment," *IEEE Access*, vol. 4, pp. 7469–7478, 2016.
[10] S. Alekseev, A. Radzievsky, I. Szabo, and M. Ziskin, "Local heating of human skin by millimeter waves: Effect of blood flow," *Bioelectromagnetics*, vol. 26, no. 6, pp. 489–501, Sep. 2005.
[11] S. Alekseev, A. Radzievsky, M. Logani, and M. Ziskin, "Millimeter wave dosimetry of human skin," *Bioelectromagnetics*, vol. 29, no. 1, pp. 65–70, Jan. 2008.
[12] M. Zhadobov, N. Chahat, R. Sauleau, C. Le Quement, and Y. Le Drean, "Millimeter-wave interactions with the human body: State of knowledge and recent advances," *Int. J. Microw. Wireless Technol.*, vol. 3, no. 2, pp. 237–247, Apr. 2011.
[13] *IEEE Standard for Safety Levels With Respect to Human Exposure to Radio Frequency Electromagnetic Fields, 0 Hz to 300 GHz*, Standard IEEE-C95.1-2019, New York, NY, USA, 2019.
[14] W. H. Bailey *et al.*, "Synopsis of IEEE Std C95.1-2019 IEEE standard for safety levels with respect to human exposure to electric, magnetic, and electromagnetic fields, 0 Hz to 300 GHz," *IEEE Access*, vol. 7, pp. 171346–171356, 2019.
[15] A. Ahlbom, U. Bergqvist, J. H. Bernhardt, J. P. Cesarini, L. A. Court, M. Grandolfo, M. Hietanen, A. F. McKinlay, M. H. Repacholi, D. H. Sliney, J. A. J. Stolwijk, M. L. Swicord, L. D. Szabo, M. Taki, T. S. Tenforde, H. P. Jammet, and R. Matthes, "Guidelines for limiting exposure to time-varying electric, magnetic, and electromagnetic fields (up to 300 GHz)," *Health Phys.*, vol. 74, no. 4, pp. 494–522, Apr. 1998.
[16] ICNIRP, "Guidelines for limiting exposure to electrromagnetic fields (100 kHz to 300 GHz)," *Health Phys.*, to be published.
[17] *IEEE Standard for Safety Levels With Respect to Human Exposure to Radio Frequency Electromagnetic Fields, 3 kHz to 300 GHz*, Standard IEEE-C95.1, New York, NY, USA, 2005.
[18] D. Funahashi, A. Hirata, S. Kodera, and K. R. Foster, "Area-averaged transmitted power density at skin surface as metric to estimate surface temperature elevation," *IEEE Access*, vol. 6, pp. 77665–77674, 2018.
[19] W. He, B. Xu, M. Gustafsson, Z. Ying, and S. He, "RF compliance study of temperature elevation in human head model around 28 GHz for 5G user equipment application: Simulation analysis," *IEEE Access*, vol. 6, pp. 830–838, 2018.
[20] D. Funahashi, T. Ito, A. Hirata, T. Iyama, and T. Onishi, "Averaging area of incident power density for human exposure from patch antenna arrays," *IEICE Trans. Electron.*, vol. E101.C, no. 8, pp. 644–646, Aug. 2018.
[21] K. Sasaki, M. Mizuno, K. Wake, and S. Watanabe, "Monte Carlo simulations of skin exposure to electromagnetic field from 10 GHz to 1 THz," *Phys. Med. Biol.*, vol. 62, no. 17, pp. 6993–7010, Jul. 2017.
[22] T. Samaras and N. Kuster, "Theoretical evaluation of the power transmitted to the body as a function of angle of incidence and polarization at frequencies >6 GHz and its relevance for standardization," *Bioelectromagnetics*, vol. 40, no. 2, pp. 136–139, 2019.
[23] D. Colombi, B. Thors, C. TöRnevik, and Q. Balzano, "RF energy absorption by biological tissues in close proximity to mmW 5G wireless equipment," *IEEE Access*, vol. 6, pp. 4974–4981, 2018.
[24] A. R. Guraliuc, M. Zhadobov, R. Sauleau, L. Marnat, and L. Dussopt, "Near-field user exposure in forthcoming 5G scenarios in the 60 GHz band," *IEEE Trans. Antennas Propag.*, vol. 65, no. 12, pp. 6606–6615, Dec. 2017.
[25] R. E. Collin, *Foundations for Microwave Engineering*. Hoboken, NJ, USA: Wiley, 2007.
[26] K. Li, K. Sasaki, S. Watanabe, and H. Shirai, "Relationship between power density and surface temperature elevation for human skin exposure to electromagnetic waves with oblique incidence angle from 6 GHz to 1 THz," *Phys. Med. Biol.*, vol. 64, no. 6, Feb. 2019, Art. no. 065016.
[27] Y. Hashimoto, A. Hirata, R. Morimoto, S. Aonuma, I. Laakso, K. Jokela, and K. R. Foster, "On the averaging area for incident power density for human exposure limits at frequencies over 6 GHz," *Phys. Med. Biol.*, vol. 62, no. 8, pp. 3124–3138, Apr. 2017.
[28] E. Neufeld, E. Carrasco, M. Murbach, Q. Balzano, A. Christ, and N. Kuster, "Theoretical and numerical assessment of maximally allowable power-density averaging area for conservative electromagnetic exposure assessment above 6 GHz," *Bioelectromagnetics*, vol. 39, no. 8, pp. 617–630, 2018.
[29] S. Gabriel, R. W. Lau, and C. Gabriel, "The dielectric properties of biological tissues: III. Parametric models for the dielectric spectrum of tissues," *Phys. Med. Biol.*, vol. 41, no. 11, pp. 2271–2293, Nov. 1996.
[30] A. Taflove and S. Hagness, *Computational Electrodynamics: The Finite-Difference Time-Domain Method*, 3rd ed. Norwood, MA, USA, 2003.
[31] H. H. Pennes, "Analysis of tissue and arterial blood temperatures in the resting human forearm," *J. Appl. Physiol.*, vol. 1, no. 2, pp. 93–122, Aug. 1948.
[32] A. Hirata, M. Morita, and T. Shiozawa, "Temperature increase in the human head due to a dipole antenna at microwave frequencies," *IEEE Trans. Electromagn. Compat.*, vol. 45, no. 1, pp. 109–116, Feb. 2003.
[33] F. A. Duck, *Physical Properties of Tissues: A Comprehensive Reference Book*. New York, NY, USA: Academic, 1990.
[34] B. Xu, K. Zhao, B. Thors, D. Colombi, O. Lundberg, Z. Ying, and S. He, "Power density measurements at 15 GHz for RF EMF compliance assessments of 5G user equipment," *IEEE Trans. Antennas Propag.*, vol. 65, no. 12, pp. 6584–6595, Dec. 2017.
[35] F. Gustrau and A. Bahr, "W-band investigation of material parameters, SAR distribution, and thermal response in human tissue," *IEEE Trans. Microw. Theory Techn.*, vol. 50, no. 10, pp. 2393–2400, Oct. 2002.
[36] P. Bernardi, M. Cavagnaro, S. Pisa, and E. Piuzzi, "SAR distribution and temperature increase in an anatomical model of the human eye exposed to the field radiated by the user antenna in a wireless LAN," *IEEE Trans. Microw. Theory Techn.*, vol. 46, no. 12, pp. 2074–2082, Dec. 1998.
[37] K. R. Foster, M. C. Ziskin, Q. Balzano, and G. Bit-Babik, "Modeling tissue heating from exposure to radiofrequency energy and relevance of tissue heating to exposure limits: Heating factor," *Health Phys.*, vol. 115, no. 2, pp. 295–307, Aug. 2018.
[38] A. Hirata, M. Fujimoto, T. Asano, J. Wang, O. Fujiwara, and T. Shiozawa, "Correlation between maximum temperature increase and peak SAR with different average schemes and masses," *IEEE Trans. Electromagn. Compat.*, vol. 48, no. 3, pp. 569–578, Aug. 2006.
[39] K. Sasaki, K. Wake, and S. Watanabe, "Measurement of the dielectric properties of the epidermis and dermis at frequencies from 0.5 GHz to 110 GHz," *Phys. Med. Biol.*, vol. 59, no. 16, pp. 4739–4747, Aug. 2014.
[40] A. Kanezaki, A. Hirata, S. Watanabe, and H. Shirai, "Effects of dielectric permittivities on skin heating due to millimeter wave exposure," *BioMed. Eng. OnLine*, vol. 8, no. 1, p. 20, 2009.
[41] A. Kanezaki, A. Hirata, S. Watanabe, and H. Shirai, "Parameter variation effects on temperature elevation in a steady-state, one-dimensional thermal model for millimeter wave exposure of one-and three-layer human tissue," *Phys. Med. Biol.*, vol. 55, no. 16, pp. 4647–4659, 2010.

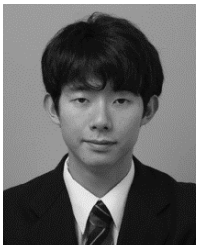

TAKUMA NAKAE received the B.E. degree in electrical and electronic engineering from the Nagoya institute of Technology, Nagoya, Japan, in 2019, where he is currently pursuing the master's degree in electrical and mechanical engineering.

DAISUKE FUNAHASHI received the B.E. degree in electrical and electronic engineering and the M.E. degree in electrical and mechanical engineering from the Nagoya Institute of Technology, Nagoya, Japan, in 2017 and 2019, respectively.

JUNJI HIGASHIYAMA (Member, IEEE) received the B.S. degree in electrical engineering and computer science from Kyushu University, Fukuoka, Japan, in 2000, and the M.S. degree in applied science for electronics and materials from the Interdisciplinary Graduate School of Engineering Sciences, Kyushu University, in 2002.

He is currently a Research Engineer with the Wireless Emerging Technology Research Group, Research Laboratories, NTT DOCOMO, Inc., Kanagawa, Japan. His current research interests include the development and standardization of evaluation methods of electromagnetic field (EMF) from mobile base stations and the study of EMC including electromagnetic interferences with medical equipment.

Mr. Higashiyama is a member of the Institute of Electronics, Information and Communication Engineers (IEICE). He is a member of the International Electrotechnical Commission (IEC) TC106 MT3.

TERUO ONISHI (Member, IEEE) received the B.S. degree in physics from the Tokyo University of Science, Tokyo, Japan, in 1987, and the Ph.D. degree from the Graduate School of Science and Technology, Chiba University, Chiba, Japan, in 2005.

He was with Toyo Communication Equipment Company, Ltd., Kanagawa, Japan, and Nippon Ericsson K.K, Tokyo, Japan. From 1990 to 1992, he worked on the Finite-Difference Time-Domain (FDTD) analysis for solving electromagnetic problems with Hokkaido University, Sapporo, Japan. He was also a Project Professor with the Nagoya Institute of Technology, Japan, from 2014 to 2017, and also a Visiting Professor with Tohoku University, Japan, in 2017. He is currently a Senior Research Engineer with the Wireless Emerging Technology Research Group, Research Laboratories, NTT DOCOMO, Inc., Kanagawa. His current research interests include the standardization of electromagnetic field (EMF) evaluation method and the study of EMC including electromagnetic interferences with medical equipment.

Dr. Onishi was a Board Member of the Bioelectromagnetics Society (BEMS), from 2016 to 2018 and a member of the Institute of Electronics, Information and Communication Engineers (IEICE). He is a Chair of the IEEE International Committee on Electromagnetic Safety (ICES) TC-34 and also conveners of the International Electrotechnical Commission (IEC) TC106 WG9 and JWG12, and a Project Leader of IEC TC106 PT63184. He received the 1906 award from the IEC in 2017.

AKIMASA HIRATA (Fellow, IEEE) received the B.E., M.E., and Ph.D. degrees in communications engineering from Osaka University, Suita, Japan, in 1996, 1998, and 2000, respectively.

From 1999 to 2001, he was a Research Fellow with the Japan Society for the Promotion of Science, and also a Visiting Research Scientist with the University of Victoria, Victoria, BC, Canada, in 2000. In 2001, he joined the Department of Communications Engineering, Osaka University, as an Assistant Professor. In 2004, he joined, as an Associate Professor with the Department of Computer Science and Engineering, Nagoya Institute of Technology, where he is currently a Full Professor. His research interests include electromagnetic safety, risk management system for heat-related illness, methods in neuroscience, antennas, filters, and related computational techniques.

Prof. Hirata is an Editorial Board Member of physics in medicine and biology, a member of the main commission and a Chair of project group of International Commission on Non-Ionizing Radiation Protection, and a member of administrative committee and a Subcommittee (EMF Dosimetry Modeling) Chair of the IEEE International Committee on Electromagnetic Safety, and an Expert of World Health Organization. He is a Fellow of the Institute of Physics, and a member of IEICE, IEE Japan, and the Bioelectromagnetics Society. He received several awards including Young Scientists' Prize in 2006 and Prizes for Science and Technology (Research Category 2011, Public Understanding Promotion Category 2014) by the Commendation for Science and Technology by the Minister of Education, Culture, Sports, Science, and Technology, Japan, and the IEEE EMC-S Technical Achievement Award in 2015, and the Japan Academy Medal and JSPS Prize in 2018. From 2006 to 2012, he was also an Associate Editor of the IEEE TRANSACTIONS ON BIOMEDICAL ENGINEERING.